 DOI: 10.1002/masy.200950806

Perfectly Controlled Lamella Thickness and Thickness Distribution: A Morphological Study on ADMET Polyolefins

S. Hosoda,[*1] *Y. Nozue,*[1] *Y. Kawashima,*[1] *S. Utsumi,*[1] *T. Nagamatsu,*[1] *K. Wagener,*[2] *E. Berda,*[2] *G. Rojas,*[2] *T. Baughman,*[2] *J. Leonard*[2]

Summary: Lamella thickness distribution (LTD) plays a critical role in determining the mechanical properties of polyethylene. LTD is predominantly governed by the intermolecular chemical composition distribution, but intrachain heterogeneity also results in a broadened LTD. Polyethylene synthesized by acyclic diene metathesis (ADMET) contains pristine microstructures free from inter and intrachain heterogeneity and therefore represent ideal models to investigate these phenomena. The crystalline structures of ADMET polyethylene with ethyl or *n*-hexyl branches every 21st backbone carbon (EB21and EO21, respectively) were characterized by transmission electron microscopy (TEM), small X-ray scattering and wide angle X-ray diffraction (SAXS and WAXD), and differential scanning calorimetry (DSC). The samples were crystallized for various periods at temperatures near the DSC crystallization peak temperatures: 10 °C for EB21 and 0 °C for EO21. TEM observation exhibited that EB21 displays straight lamellar crystals with axialitic organization and an average thickness of about 55 Å. This corresponds to twice the ethylene sequence length between branches, suggesting that one lamellar stem spans three branches and includes one ethyl branch within the lamella. The lamella thickness distribution was very narrow compared with that of the cross-fraction of ethylene/1-butene copolymer prepared via Ziegler-Natta polymerization. Similarly it was found from the same characterization methods that EO21 also displays a narrow lamella thickness distribution albeit with thinner lamellae, averaging 25–26Å thick. Judging from this lamella thickness, EO21 is considered to have a lamella stem composed of a single ethylene sequence between two braches, suggesting that the *n*-hexyl branch is entirely excluded from a crystalline phase.

Keywords: ADMET polyethylene; branch inclusion; ethylene sequence length; lamella crystal; lamella thickness distribution; TEM

Introduction

When attempting to elucidate the relationship between the structure and properties of polyethylene, certain structural factors and their distributions must be considered. From this viewpoint, polyethylenes prepared via acyclic diene metathesis (ADMET) are ultimate models that have perfectly regular placement of short chain branching (SCB). In order clarify the meaning of this precisely structured polyethylene it is necessary review the molecular structure-crystalline structure relationships including their distributions, and structure-property relationships of the ethylene/α-olefin copolymers possessing structural heterogeneities.

[1] Sumitomo Chemical Co. Ltd., Petrochemicals Research Laboratory, Kitasode 2-1, Sodegaura-city, Chiba, 299-0295, Japan
E-mail: hosodas@sc.sumitomo-chem.co.jp
[2] The George and Josephine Butler Polymer Research Laboratory, University of Florida, Department of Chemistry, Gainesville, FL, 32611, USA

Copyright © 2009 Wiley-VCH Verlag GmbH & Co. KGaA, Weinheim

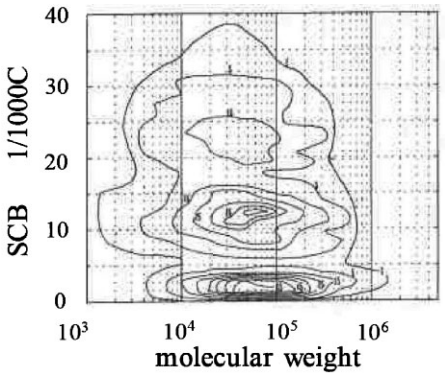

Figure 1.
Typical molecular structure distribution of LLDPE prepared with Ziegler-Natta catalyst.[5]

Intermolecular Structure Distribution

The heterogeneity of the LLDPE structure has been characterized by various fractionation techniques.[1–6] As shown in Figure 1, LLDPE prepared with a heterogeneous catalyst systems such as those utilized in Ziegler-Natta polymerizations generally exhibit a wide intermolecular structural distribution.[5] The component with the highest molecular weight and least comonomer content is common to every LLDPE of this type. Depending on the catalysts and polymerization processes, we can see the second and third component separately, like the sample in this figure. However, there are a variety of LLDPEs commercially produced by an assortment of catalyst systems and polymerization processes, so LLDPEs showing the second and third component separately are rather minor and most of them exhibit a broad second component. In crystallization they make their own lamellar crystals fundamentally, leading to the heterogeneous lamella morphology shown in Figure 2.[7] Two different types of lamellae are observed in this figure. One is thick and growing straight; while the other is thin and very short, as if it is formed parasitically on the straight one. The area-based lamella thickness distribution (LTD) clearly suggests that the LTD of this LLDPE is very broadly spread from 50 to 170 Å.

This is typically attributed to the broad intermolecular composition distribution of LLDPE and is confirmed by morphology observation of cross fractions of the molecular weight fraction.[7] On the other hand, LLDPEs polymerized by homogeneous catalysis such as a metallocene/MAO system exhibit a narrow intermolecular structural distribution and thus give a narrower lamella thickness distribution than that of an LLDPE obtained with heterogeneous catalyst systems.[8,9]

Intramolecular Structure Distribution and Short Chain Branching

Compared with the number of papers on the intermolecular structural distribution of

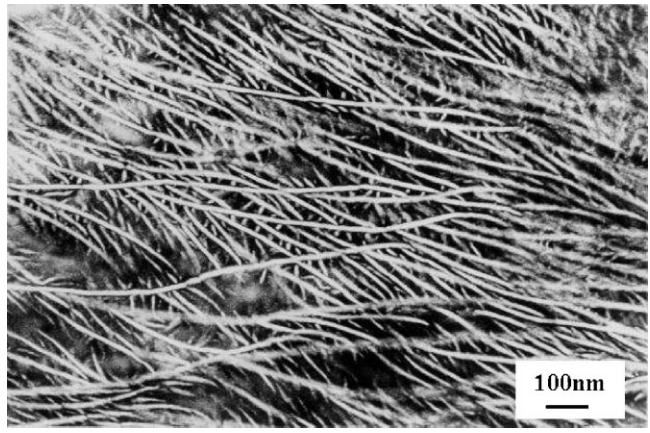

Figure 2.
Typical lamella morphology of LLDPE (A) fraction prepared with Ziegler-Natta catalyst (C'2/C'4-1, Mw = 8.8×10^4, d = 0.919g/cm³).[7]

Copyright © 2009 Wiley-VCH Verlag GmbH & Co. KGaA, Weinheim

LLDPE, there are only a few on intrastructure distribution. The location of SCB in LLDPEs is not considered regular due to the inherent, sometimes blocky distribution of comonomer along the polymer chain ultimately governed by the monomer reactivity ratio. ^{13}C-NMR spectroscopy has revealed the blockiness of comonomer location in various kinds of ethylene copolymers.[10–14] The effect of the ethyl branch randomness on the crystallinity and melting point can be detected using cross fractions of ethylene/1-butene copolymers.[5] The fractions with blocky ethyl distribution show a higher crystallinity and higher melting temperature than the fractions of higher randomness, indicating that the long ethylene sequences result in thicker lamellae. Mirabella states,[15] on the basis of statistical treatment, that blockiness has more effect on the melting temperature of ethylene copolymers than an alternating character. This result suggests at the same time that the comonomer sequence distribution leads to the lamella thickness distribution even in the case of cross fractions or homogeneously catalyzed copolymers that have very narrow intermolecular structure distribution. By correlating DSC data with direct observation using an atomic force microscopy (AFM), Mirabella determined that ethylene copolymers with a homogeneous intermolecular composition distribution also possess a broad lamella thickness distribution.[16–18] The broadening of the lamella thickness distribution was estimated to occur as a result of stepwise lamella growth based on the ethylene sequence length distribution.

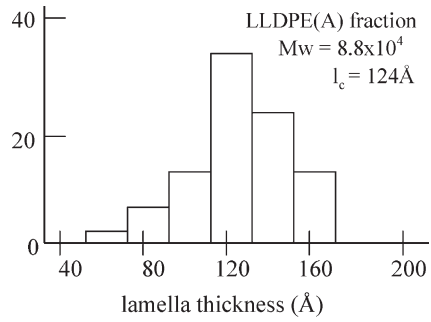

Figure 3.
Lamella thickness distribution of LLDPE Figure (A) fraction by TEM observation.[7]

Furthermore, SCB species are considered to be very important in determining the crystallinity, lamella thickness, and lamella thickness distributions through their inclusion in the crystalline phase. Among samples of the same degree of sequence randomness, we can evaluate the degree of SCB inclusion in the crystalline phase by various methods.[19–34] The absolute value of the inclusion tendency for each kind of SCB is very difficult to obtain, however, because of the sequence length distribution based on the statistics of SCB randomness. Therefore copolymers without a sequence distribution would allow clarification as to whether or not a SCB could be included.

Mechanical Properties and Lamella Thickness Distribution

Concerning the effect of structure and morphological factors on the properties, studies were carried out using ethylene/α-copolymers and hydrogenated polybutadiene.[35–41] To access the effect of the lamella thickness distribution on the mechanical properties of LLDPE, we measured the mechanical strength of the molecular weight fractions of various molecular weights.[42] Our findings indicate that mechanical properties such as tensile impact strength are governed by the lamella thickness distribution regardless of the kind of comonomer. More simply stated a narrower lamella thickness distribution results in higher impact strength.[42] This relationship can be explained from the viewpoint of tie molecule concentration and its orientation in deformation. Both the experimentally obtained tie molecular orientation[8,43] and the tie molecule probability[42,44,45] calculated from the method of Huang and Brown[46] show a convex type of dependence on crystallinity and they exhibited maximum value at the crystallinity of 40–50%. It is reasonable to consider how many tie molecules of the same degree of orientation existing in a

Copyright © 2009 Wiley-VCH Verlag GmbH & Co. KGaA, Weinheim

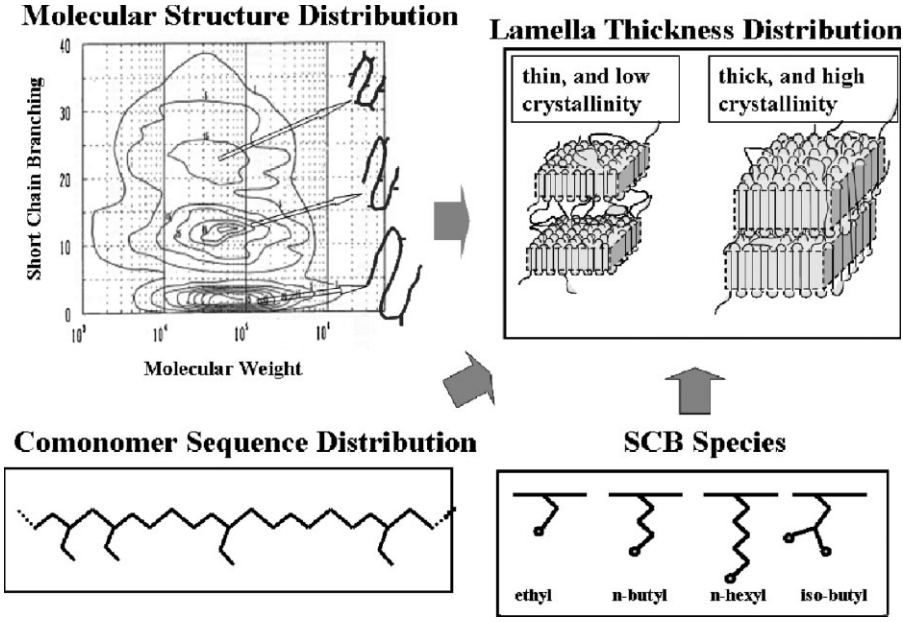

Figure 4.
Relationships among inter- and intra-molecular structural distributions, short chain branching spiecies, and the lamella thickness distribution.

deformed state strongly influence the mechanical strength of polyethylene. Consequently, homogeneity of the crystallinity and lamella thickness should increase the percentage of actually efficient tie molecules. Figure 5 shows a deformed state model of two typical samples that have the same molecular weight, the same crystallinity and the different lamella thickness distribution.[9,44] When loaded, the external force is concentrated on tie molecules. The load on each tie molecule is different between two samples. It is easy to visualize that the upper sample with homogeneous lamella thickness distribution clearly possesses advantage in mechanical strength compared to the heterogeneous case.

The aim of this study was to further elucidate the relationship between the homogeneity of structure on the molecular

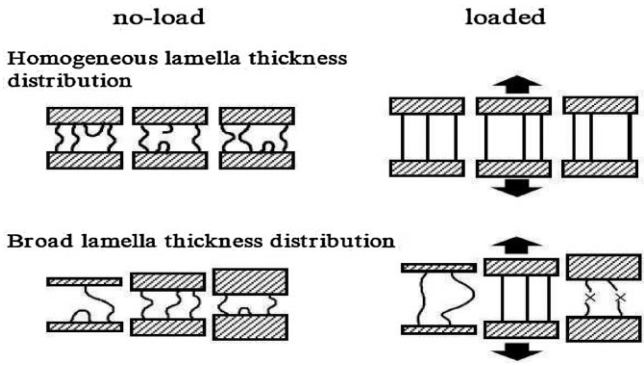

Figure 5.
Schematic representation of deformation of LLDPE with the different lamella thickness distribution[9,44]

Copyright © 2009 Wiley-VCH Verlag GmbH & Co. KGaA, Weinheim

level and the thickness and also thickness distribution of crystalline lamella for ethylene/α-olefin copolymers. In this light, polyethylene without intermolecular or intramolecular heterogeneities is of a great interest from the viewpoint of crystalline structure homogeneity. We therefore studied the morphology of precisely short-chain-branched polyethylenes prepared by ADMET polycondensation and subsequent hydrogenation.[47–54] The samples used here contain ethyl or *n*-hexyl branches on every 21st backbone carbon (EB21 and EO21, respectively).

Experimental Part

Materials

ADMET polyethylenes, EO21 and EB21, were synthesized as previously described.[48,50] Weight average molecular weights measured by size exclusion chromatography are 33,000 for EB21 and 40,000 for EO21. Polydispersity indices (M_w /M_n) are 1.6 (EB21) and 2.0 (EO21), respectively. EB21 possesses ethyl and EO21 *n*-hexyl branches every 21st backbone carbon; the degree of alkyl branch is then 48 / 1000C for both samples.

TEM Observation

Both of EB21 and EO21 were mounted in epoxide resin to treat them easily and stored in water at 50 °C in a glass beaker. They were then cooled down to the temperature of crystallization by two methods. In the case of quenching, samples were rapidly transferred into water kept at the crystallization temperature. In a slowly cooled condition, samples stored in water at 50 °C were transferred into a refrigerator that was kept at the crystallization temperature. Both kinds of cooling conditions and their average cooling rate, measured with a thermocouple, are shown below.

Table 1.
Sample preparation conditions for TEM observation.

Cooling from 50 °C to	Cooling Rate (°C /min)	
	Quenched	Slowly cooled
10 °C (EB21)	−14	−1
0 °C (EO21)	−46	−0.07

EB21 was crystallized at 10 °C for one hour, one day and four days, respectively, and then stained with the vapor of an aqueous solution of RuO_4 (1 wt%). EO21 was crystallized at 0 °C for the same periods as those of EB21 prior to staining. Staining was carried out at each crystallization temperature for three days. Therefore crystallization might proceed during the initial stage of the staining process until the amorphous phase is fixed with RuO_4 and the molecular movement is intrinsically restricted. It is vague as to how long is necessary to fix the amorphous phase by RuO_4 vapor and to retard the further crystallization, but the amorphous phase is supposed to be fixed very rapidly by RuO_4 vapor, judging from the time conversion curves of oxidative products reported by Sano et al.[55] The stained samples were sectioned using ultra microtome under liquid nitrogen vapor atmosphere. Sections were collected on 300 mesh copper grids and TEM observation was conducted at room temperature with a HITACHI H-8000 transmission electron microscope under the accelerating voltage of 200 kV. Lamella thickness distribution was obtained by counting the thickness and the length of more than 100 lamellae. The counting process was carried out two times by different people to enhance the reliability of the results. Distribution was expressed as an occupied area-based fraction. Thickness was counted for every 4 Å division and two divisions were included into one scale.

X-ray Diffraction Measurements

WAXD and SAXS were performed on a Nanoviewer X-ray system equipped with RA-Micro7 (Rigaku Co. Ltd.) using Cu Kα radiation. Sample temperature was controlled by LINKAM hot stage during X-ray measurements. X-ray crystallinity was determined by subtracting the amorphous halo that was measured at 50 °C from WAXD total diffractogram. Long period

Copyright © 2009 Wiley-VCH Verlag GmbH & Co. KGaA, Weinheim

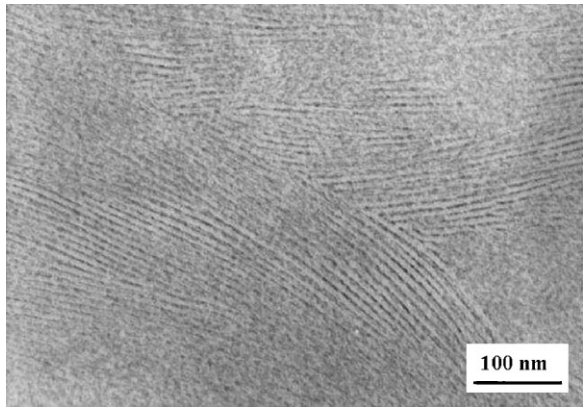

Figure 6.
TEM observation of lamella crystalline morphology of ADMET-PE EB21 slowly cooled and crystallized at 10 °C for four days.

was evaluated by circularly averaged SAXS profile.

Differential Scanning Calorimetry

Melting and crystallization behavior during heating and cooling were measured by a DSC6200 (Seiko Instrument Inc.). The thermal history is as follows; sample is melted at 70 °C, cooled at the rate of 10 °C/min to -40 °C, and heated at 10 °C/min. The system was calibrated with an indium standard. Melting behavior after pseudo-isothermal crystallization, which corresponds to the condition of sample preparation for TEM observation, was measured as follows. A DSC pan containing sample (ca. 5mg) was kept at 50 °C for 10 min and was transferred into a temperature controllable apparatus (TRL108H, Thomas Kagaku Co. Ltd.). The pan was cooled at the rate of 0.1 °C /min to the crystallization temperature (10 °C for EB21 and 0 °C for EO21), then kept for three days at that temperature. After crystallization, the pan was quickly transferred into the DSC that was set at 0 °C for EO21 or 5 °C for EB21. Then, the DSC trace was recorded at 5 °C /min.

Results and Discussion

Morphology Observation with TEM

Figure 6 shows the TEM image of EB21 prepared under a slow cooling and crystallized at 10 °C for four days. Lamellar stacks with an axialitic organization are observed over the entire image. Long and straight lamellae are dominant, and straight lamellae propagate to lengths of almost one micron. Spherulitic or twisted lamellae, the common morphologies of LLDPEs,[7] were not observed even at lower magnification. Figure 7 exhibits the lamella thickness distributions for (a) EB21 prepared under a quenched condition and kept for one day at 10 °C, and (b) the cross-fraction of ethylene/1-butene LLDPE prepared via Ziegler-Natta polymerization (melt-crystallized quenched sample [7]). The diagram (b) was reproduced from a figure in the original paper [7] to compare two diagrams on the same horizontal scale. The term 'cross fraction' here means the fraction that was obtained by a temperature-rising elution fractionation (TREF) of the molecular weight fraction, and therefore it has an especially narrow intermolecular distribution in terms of both chemical composition and molecular weight. Though the lamella thickness distribution of the cross-fraction is clearly narrower than the sample before cross fractionation, as seen in the original paper, the distribution in Figure 7b seems rather wide compared with EB21 (Figure 7a). The cross fraction does not have a substantial intermolecular chemical composition distribution, but it generally possesses an intramolecular distribution (ethylene

Copyright © 2009 Wiley-VCH Verlag GmbH & Co. KGaA, Weinheim

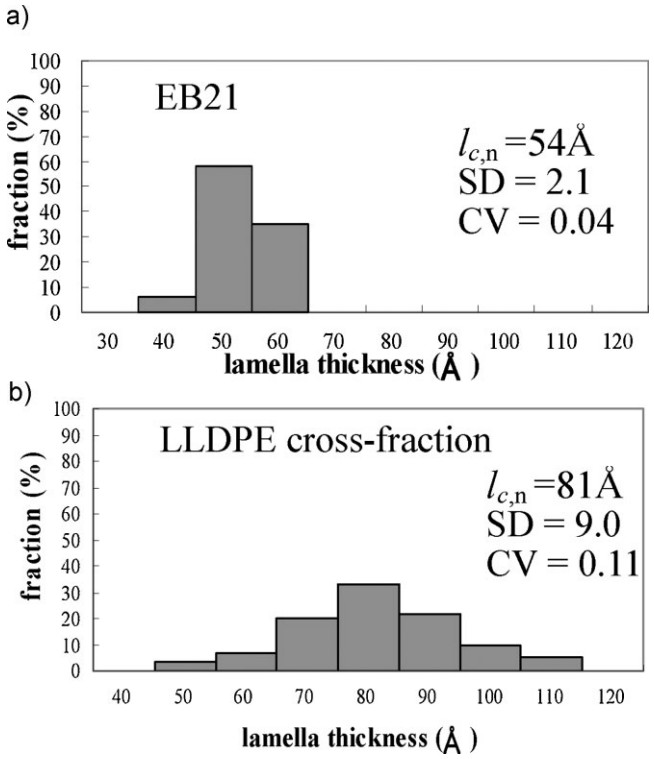

Figure 7.
Lamella thickness distribution of (a) EB21(quenched and kept at 10 °C for one day), and (b) LLDPE cross fraction (Mw = 88K, M_w/M_n = 1.2, ethyl = 22.3/1000C).

sequence length distribution) as long as the sample is prepared via the chain addition copolymerization process. Actually, it was proven by ^{13}C-NMR spectroscopy that the cross-fraction used here has a blocky tendency in terms of the ethyl branch positions.[5] Mirabella first indicated from DSC analysis that even LLDPE with a sharp composition distribution makes a broad lamella thickness distribution due to intrachain heterogeneity,[16] and then revealed via *in situ* AFM observation that sequential step crystallization occurs due to the different ethylene sequence lengths.[16,17] Considering the results above, a wide lamella thickness distribution of the cross-fraction in Figure 7b is seemingly due to the random ethylene sequence length distribution of the cross-fraction. On the other hand, EB21 shows a very narrow lamella thickness distribution as seen in the standard deviation (SD) and the coefficient of variation (CV) by which the comparison between samples of different average values is available. The difference in lamella thickness distribution between the two samples might be due to the difference in the ethylene sequence length distribution, a product of the polymerization method (olefin chain-addition copolymerization versus ADMET polycondensation).

The lamella thickness distributions for the EB21 samples prepared under various conditions are exhibited in Figure 8. All the distributions are narrow, and the effect of the preparation conditions (quenched or slowly cooled) does not seem significant in this sample. The average lamella thickness of 55Å is about double the ethylene sequence length between ethyl branches, suggesting that one ethyl branch has to be included into each lamella stem.

Figure 9 shows TEM micrograph of EO21. It is observed that EO21 makes

Copyright © 2009 Wiley-VCH Verlag GmbH & Co. KGaA, Weinheim

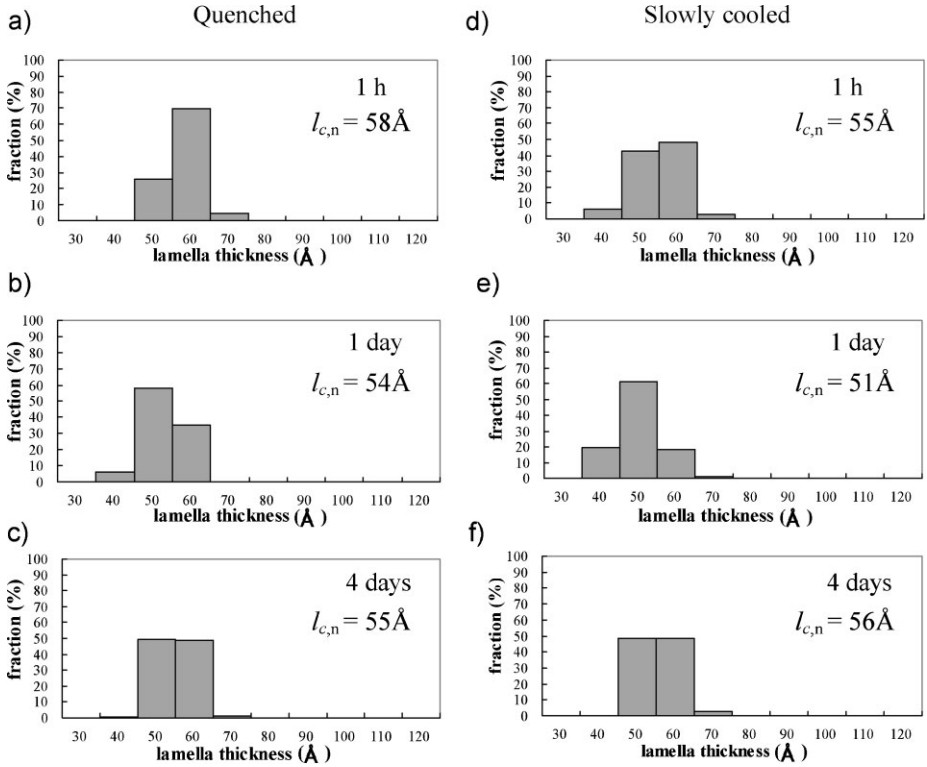

Figure 8.
Lamella thickness distributions of EB21; Cooling condition and crystallization period; (a), (b), (c); quenched, (d), (e), (f); slowly cooled, (a), (d); one hour, (b), (e); one day, (c), (f); four days.

lamellar stacked crystals with axialitic organization like EB21, but it is obvious that EO21 makes thinner lamellae than EB21. The initial cooling rate and annealing period at 0 °C were changed and the lamella thickness distribution of each sample was measured (Figure 10). A narrow distribution was observed for every run of EO21. As shown in Figure 10, the number average lamella thickness ($l_{c,n}$) was calculated to be

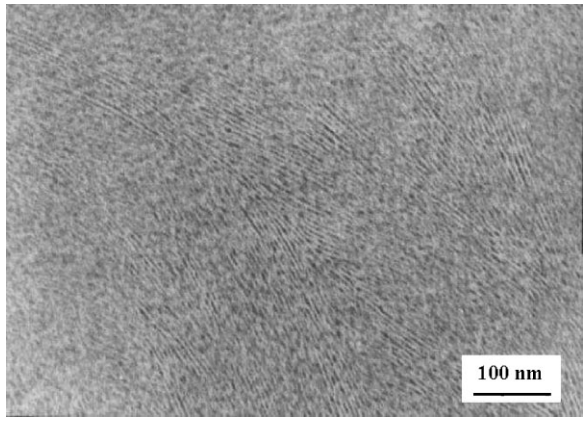

Figure 9.
TEM observation of ADMET-PE EO21 slowly cooled and crystallized at 0 °C for four days.

Copyright © 2009 Wiley-VCH Verlag GmbH & Co. KGaA, Weinheim

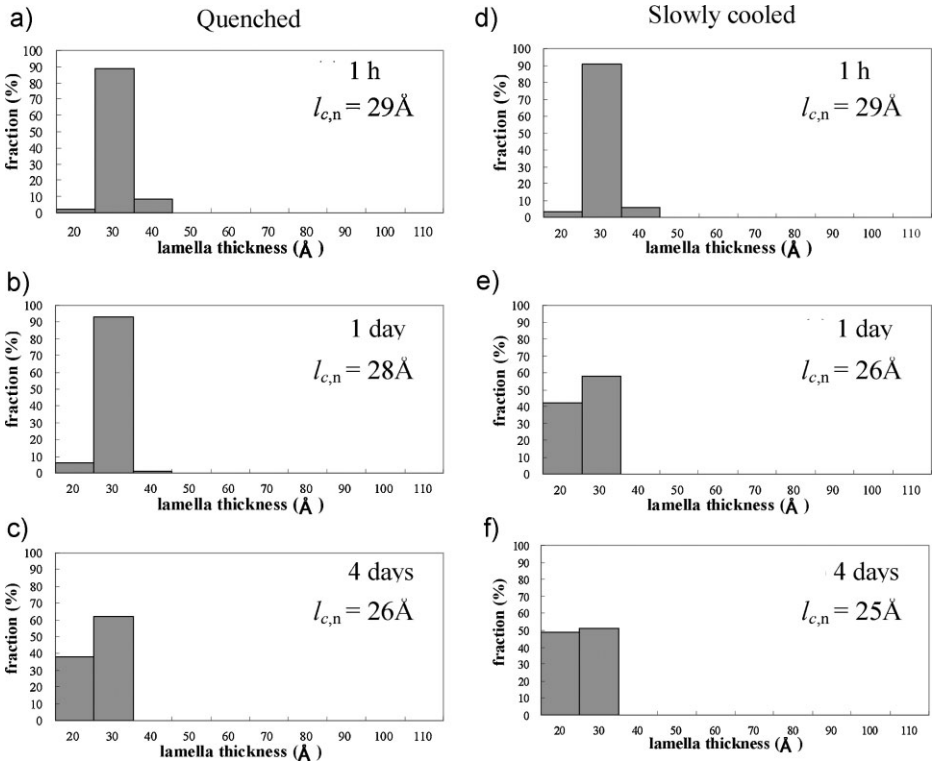

Figure 10.
Lamella thickness distributions of EO21; Cooling condition and crystallization period; (a), (b), (c); quenched, (d), (e), (f); slowly cooled, (a), (d); one hour, (b), (e); one day, (c), (e); four days,

25–29 Å. This $l_{c,n}$ decreases with increasing the length of annealing period, though the absolute value of change is small. The $l_{c,n}$ after annealing for four days corresponds to the distance between consecutive *n*-hexyl branches in the CH_2 sequence (25.4 Å), and thus gives us presumptive evidence of *n*-hexyl branch exclusion from the lamella stem. Thicker lamellae (40 Å) observed in samples annealed for one hour disappeared after annealing for longer periods, while the population of lamellae with medium thickness (30–40 Å) gradually decreased concurrent with an increase in population of thinner lamellae (20–30 Å). These results can be explained by the presence of metastable crystals which include the *n*-hexyl branch in their crystalline stem that reorganize during the annealing process forming more stable, thinner crystals by excluding the branch into the amorphous phase.

Characterization with WAXD and SAXS

Small-angle X-ray scattering (SAXS) patterns of EB21 and EO21 prepared under quenched or slowly cooled conditions and kept at their crystallization temperature for four days are shown in Figures 11 and 12. EB21 (Figure 11) exhibits two different scattering peaks corresponding to long periods of 84Å and 34Å for quenched samples, and 80Å and 37Å for slowly cooled samples. On the other hand, SAXS patterns of EO21 exhibit a sharp single scattering peak at long periods of 41Å both for quenched and slowly cooled samples as shown in Figure 12, suggesting the narrow distribution of a higher structural ordering. Furthermore, the cooling rate from the melt to the crystallization temperature (0 °C) seems to affect the long period distribution, as observed by the difference of the peak half width; i.e., slow cooling gives a narrower distribution of the long period than the quench cooling.

Copyright © 2009 Wiley-VCH Verlag GmbH & Co. KGaA, Weinheim

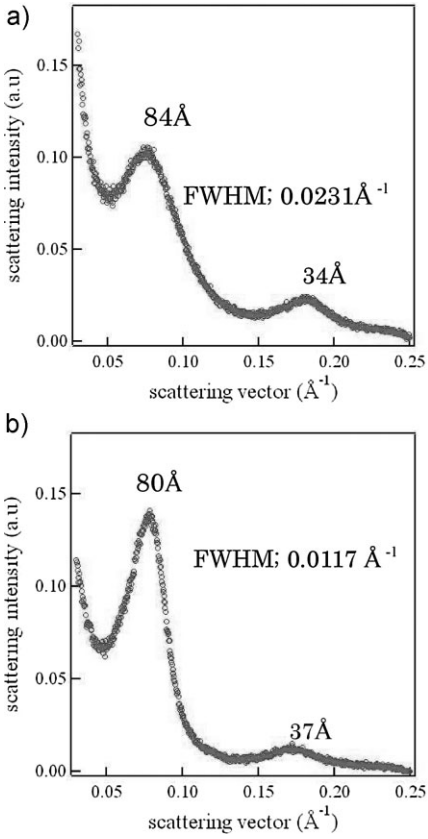

Figure 11.
SAXS pattern of EB21 crystallized at 10 °C for four days. Cooling condition; (a) quenched, (b) slowly cooled.

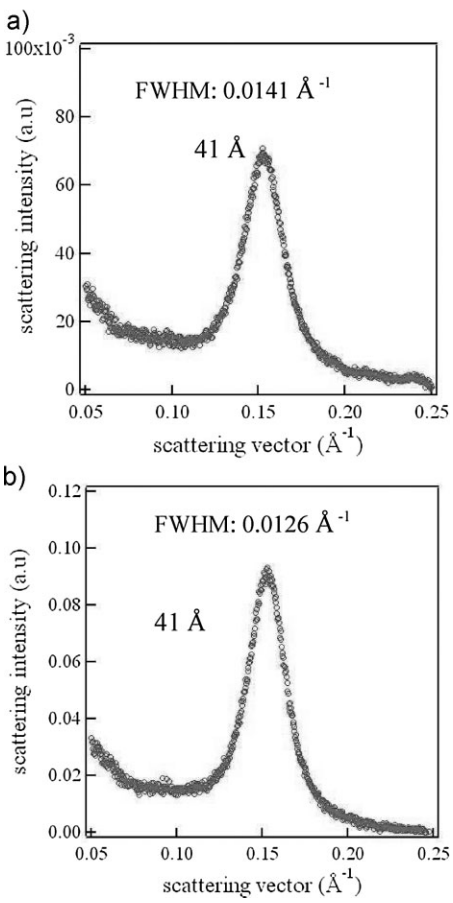

Figure 12.
SAXS pattern of EO21 crystallized at 0°C for four days. Cooling condition; (a) quenched, (b) slowly cooled.

Figure 13 shows wide-angle X-ray diffraction (WAXD) patterns of EB21, having the same thermal histories as the SAXS samples above. EB21 exhibits reflection peaks at 20.2° and 22.5°. Qui et al. [49] reported a triclinic structure having a tendency to be (pseudo) hexagonal for EB21 from a WAXD pattern that showed the main peak at 19.6° with a minor one at 21.7°. The peak position and relative intensity of EB21 in Figure 13 do not match either Qui's result or any reported result of a polyethylene WAXD measurement, but the main and prominent peak at 20. 2° accompanied by a minor reflection at 22.5° indicates a dominant hexagonal structure pointing to a triclinic tendency for EB21. A hexagonal structure is reasonably assumed from the a-axis expansion due to a regular ethyl inclusion in the crystalline lattice of EB21. If the ethyl branches included were aligned horizontally on the same plane in the crystal, the lattice would be crowded with ethyl branches, likely causing an unstable state. Therefore, it is reasonable that ethyl branches in the crystal would be staggered to avoid too much distortion of the lattice. This arrangement leads to a-b plane tilting at a reasonable angle to the CH_2 sequences (c-axis), resulting in a triclinic tendency. In halogen containing ADMET-PE, Alamo et al.[56] proposed that the plane formed by Cl atoms that are included in the crystal is tilted about 55° with respect to the chain axis for Cl substituted ADMET-PE (chlorinated on every ninth backbone carbon; PE9Cl).

Copyright © 2009 Wiley-VCH Verlag GmbH & Co. KGaA, Weinheim

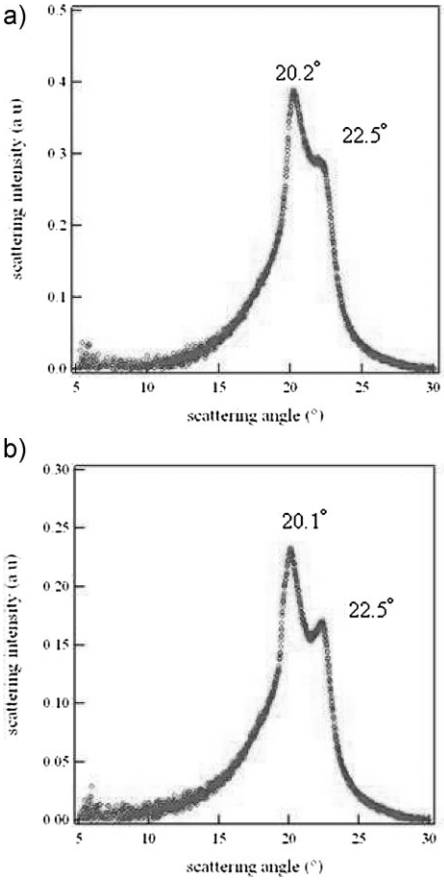

Figure 13.
WAXD pattern of EB21 crystallized at 10°C for four days. Cooling condition; (a) quenched, (b) slowly cooled.

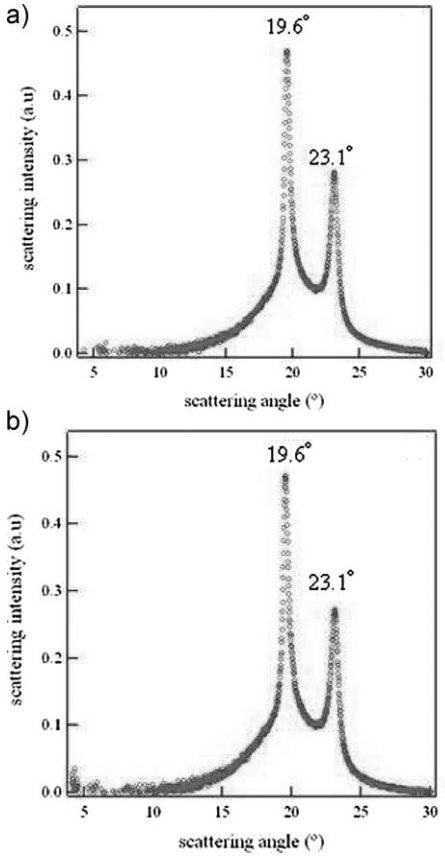

Figure 14.
WAXD pattern of EO21 crystallized at 0°C for four days. Cooling condition; (a) quenched, (b) slowly cooled.

The WAXD pattern for EO21 (Figure 14) exhibits sharp reflections at 19.6°and 23.1°. Judging from the results of the monoclinic polyethylene diffractions (19.45° and 23.17°)[57,58] and from a report on another EO21sample,[59] this pattern is considered to be associated with monoclinic packing, where the reflections at 19.6°and 23.1°correspond to planes (001) and (200), respectively. The d-spacing calculated from the two reflections are 7.67Å for a-axis and 4.56Å for c-axis. An analogous methyl-branched ADMET-PE (EP21)[49] was reported to have a monoclinic arrangement also exhibiting diffraction peaks of the (001) and (200) plane observed at 19.1° and 22.1°, respectively. The shift to a lower angle compared with monoclinic polyethylene was explained as a result of a lattice expansion due to methyl branch accommodation as a crystalline defect. Intriguingly, this suggests that the *n*-hexyl in EO21 does not affect the lattice dimensions at all due to the complete exclusion from the crystalline phase.

The average lamella thickness by TEM observation and X-ray data for the same samples (quenched and crystallized for four days) are gathered in Table 2. The lamella thickness calculated from the long period and crystallinity is comparable with that from TEM observation, especially for EO21. The last column is the CH_2 sequence

Copyright © 2009 Wiley-VCH Verlag GmbH & Co. KGaA, Weinheim

Table 2.
Characteristic data of EB21 and EO21 quenched and crystallized for four days.

Sample	TEM	SAXS	WAXD	L * Xc	Sequence length
	l_c(Å)	L (Å)[a]	X_c (%)[b]	l_c (Å)	l_c (Å)
EB21	55	84	54	45	(d) 52.4
EO21	26	41	56	23	(s) 25.4

a) long period, b) volume % crystallinity.
Crystallization temp.; 10 °C for EB21 and 0 °C for EO21.

length calculated by supposing that the CH_2's are in an all *trans* zigzag conformation in the crystal. The single-sequence length is 25.4 Å and the double-sequence length is 52.4 Å. It is very interesting that the average lamella thickness from TEM observation is very close to the CH_2 sequence length – a single sequence for EO21 and a double-sequence length for EB21. These results, showing that EB21 makes the lamella equal to a double-sequence length provides evidence for ethyl branch participation in the crystalline stem, while the data demonstrating that EO21 makes a single-sequence length crystal suggests the complete exclusion of the *n*-hexyl branch from the crystalline stem.

Thermal Behavior by DSC Measurements

The DSC curves for EB21 and EO21 are shown in Figure 15. Both samples show very sharp melting endotherms like that of high-density polyethylene (homo polyethylene) regardless of the lower peak melting temperatures. Typical metallocene-catalyzed ethylene/1-butene (ethyl; 59/1000C) and ethylene/1-octene (n-hexyl; 54/1000C) copolymers exhibit broad melting transitions ranging from 3 to 75 °C with heats of fusion between 22-32 mJ/mg. On the contrary EB21 melts in a narrow range from 12 to 26 °C with a heat of fusion of 67 mJ/mg; EO21 from 0 to 16 °C and 55 mJ/mg (both samples; 48 SCB/1000C). This suggests a different crystallization process between ADMET-PE and the copolymers of ethylene/α-olefin with a narrow intermolecular composition distribution. For the copolymers, crystallization should occur preferentially in longer CH_2 sequences within the sequence length distribution first, while ADMET PE chains crystallize in a narrow temperature window due to a lack of inter and intrachain heterogeneity.

The DSC curves of the samples crystallized at 10 °C (EB21) and 0 °C (EO21) for three days are shown in Figure 16. These crystallization conditions are similar to those of the samples for TEM observation. The T_m of EB21 increased by ca. 13 °C under isothermal crystallization compared with the T_m measured under the normal condition (cooling and heating at the rate of 10 °C /min), while EO21 did not show such a large increase. The difference in the heating curves of EB21 under two different crystallization conditions seems to indicate that the crystals formed during cooling at 10 °C /min are metastable. More stable crystals are formed during cooling the

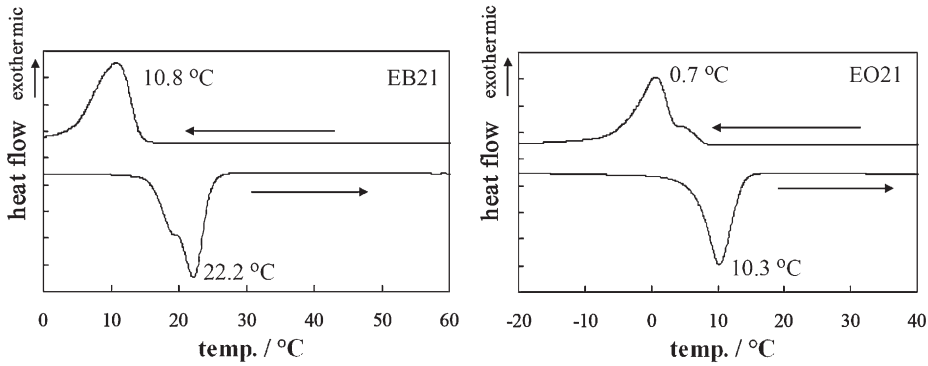

Figure 15.
DSC cooling and heating traces of EB21 and EO21 measured at the rate of 10 °C/min.

Copyright © 2009 Wiley-VCH Verlag GmbH & Co. KGaA, Weinheim

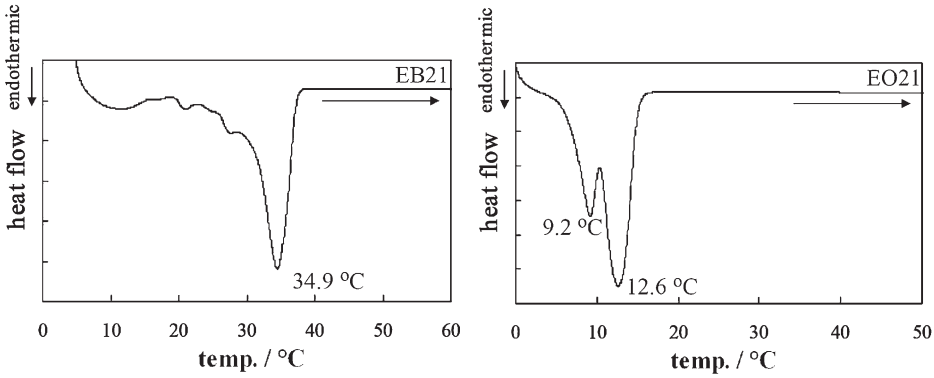

Figure 16.
DSC endothermic curves of EB21 and EO21 slowly cooled and crystallized at 10 °C (EB21) and 0 °C (EO21) for three days. Heating rate is 5 °C /min.

sample at the rate of 0.1 °C /min and annealing at the crystallization temperature for three days. This would be related to the process of a kink structure reformation and ethyl branch packing into an optimum form in the crystalline stems. It was found from fuming nitric acid etching followed by ^{13}C-NMR[31] and solid state NMR[33,34] that the bulkier the branch is, the less branch inclusion in the crystalline phase occurs for random copolymers of ethylene and α-olefin. Mirabella[15] reported that there are negligible differences in sequence distribution of Ziegler-Natta and metallocene copolymers, but the influence of sequence distribution in chain addition copolymers has remained unclear in precedent studies. Since EB21 and EO21 have no intermolecular or intramolecular heterogeneity of SCB, the T_m difference between the two samples is considered exclusively due to the difference in the type of branch. The branch that can be included easily in the crystalline phase without significantly increasing the inner free energy of the crystal can make thicker lamellae, resulting in a higher peak melting temperature.

Conclusion

The mechanical properties of polyethylene are strongly related to the distribution of lamellar thickness: a narrow lamella thickness distribution results in increased tensile and impact strength. Inter and intrachain heterogeneity is considered to play a crucial role in determining the lamella thickness distribution. Previous work in this area has relied on materials produced by methods inherently subject to such inter and intrachain heterogeneities. In this report we studied model polyethylenes synthesized by ADMET polycondensation chemistry, materials that are free from these heterogeneities. The polymers studied here possess ethyl (EB21) or *n*-hexyl (EO21) branches every 21st backbone carbon. TEM observations indicate that both materials possess extremely narrow lamella thickness distributions; a result consistent with SAXS and WAXD measurements. In the case of EB21 the average lamella thickness was 55Å, roughly double the distance between ethyl branches on the backbone. This indicates that one ethyl branch must be included within the lamella stem. For EO21 the average lamella thickness was approximately 26Å, precisely the distance between *n*-hexyl branches along the backbone. This result confirms that the *n*-hexyl branch must be completely excluded from the crystalline lamella. These results highlight the ability of ADMET chemistry to produce structures highly ordered on multiple hierarchical levels. In displaying that the *n*-hexyl branch

Copyright © 2009 Wiley-VCH Verlag GmbH & Co. KGaA, Weinheim

is entirely excluded from the crystal we have proven that by controlling the sequence length between branches with significant steric requirements it is possible to precisely tune the thickness of crystalline lamella. We hope that spacing such branches further apart will impart these materials with highly controllable mechanical properties superior to any current commercial material.

[1] K. Shirayama, T. Okada, S. Kita, *J. Polym. Sci.* **1965**, *A3*, 907.
[2] L. Wild, T. Ryle, *Polymer Preprint Am. Chem. Soc.*, **1977**, *18*, 182.
[3] S. Nakano, Y. Gotoh, *J. Appl. Polym. Sci.* **1981**, *26*, 4217.
[4] F. Mirabella, Jr., E. Ford, *J. Polym. Sci. Polym. Phys. Ed.*, **1987**, *25*, 777.
[5] S. Hosoda, *Polymer J.* **1988**, *20*, 383.
[6] M. Aoyagi, Y. Sato, S. Hosoda, A. Uemura, *Bull. Inst. Chemical Research, Kyoto Univ.* **1991**, *69*, 177.
[7] S. Hosoda, k. Kojima, M. Furuta, *Makromol. Chem.* **1986**, *187*, 1501.
[8] S. Hosoda, A. Uemura, Y. Shigematsu, I. Yamamoto, K. Kojima, "*Catalyst Design for Tailor-made Polyolefins*", K. Soga, M. Terano, Eds., Kodansha, Tokyo 1994, p. 365.
[9] K. Chikanari, S. Hosoda, "*New Trends in Polyolefin Science and Technology*", S. Hosoda, Ed., Research Signpost, India 1996, p. 153.
[10] J. Randall, *J. Polym. Sci., Polym. Phys. Ed.*, **1973**, *11*, 275.
[11] E. Hsieh, J. Randall, *Macromolecules* **1982**, *15*, 353.
[12] E. Hsieh, J. Randall, *Macromolecules* **1982**, *15*, 1402.
[13] K. Kimura, T. Shigemura, S. Yuasa, *J. Appl. Polym. Sci.* **1984**, *29*, 3161.
[14] K. Kimura, S. Yuasa, Y. Maru, *Polymer* **1984**, *25*, 441.
[15] F. Mirabella, B. Crist, *J. Polym. Sci., Polym. Phys. Ed.*, **2004**, *42*, 3416.
[16] F. Mirabella, *J. Polym. Sci., Polym. Phys. Ed.*, **2001**, *39*, 2800.
[17] F. Mirabella, *J. Polym. Sci., Polym. Phys. Ed.*, **2006**, *44*, 2369.
[18] F. Mirabella, *J. Appl. Polym. Sci.* **2008**, *108*, 987.
[19] P. Swan, *J. Polym. Sci.* **1962**, *56*, 409.
[20] K. Shirayama, S. Kita, H. Watabe, *Makromol. Chem.* **1972**, *151*, 97.
[21] B. Calleja, F. González, J. Ortega, M. Salazar, *Polymer*, **1978**, *19*, 1094.
[22] G. Patel, A. Keller, E. Muetuscelli, *J. Polym. Sci., Polym. Phys. Ed.*, **1975**, *13*, 2281.
[23] R. Palmer, A. Cobbold, *Makromol. Chem.* **1964**, *74*, 174.
[24] P. Holdworth, A. Keller, *Makromol. Chem.* **1969**, *125*, 82.
[25] Y. Maeda, H. Kanetsuna, *Polymer J.*, **1981**, *13*, 357.
[26] M. Shida, H. Fisher, I. Stone, *Polym. Lett.* **1966**, *4*, 347.
[27] M. Cagiao, D. Rueda, F. B. Caleja, *Polym. Bull.* **1980**, *3*, 305.
[28] P. Holdsworth, A. Keller, *Makromol. Chem.* **1969**, *125*, 82.
[29] E. Perez, D. VanderHart, B. Chris, P. Howard, *Macromolecules* **1987**, *20*, 78.
[30] D. MacFaddin, K. Russel, E. Kelusky, *Polym. Commun.* **1988**, *29*, 258.
[31] S. Hosoda, H. Nomura, Y. Gotoh, H. Kihara, *Polymer*, **1990**, *31*, 1999.
[32] S. Hosoda, H. Hori, K. Yada, S. Nakahara, M. Tsuji, *Polymer*, **2002**, *43*, 7451.
[33] R. Alamo, D. VanderHart, M. Nyden, L. Mandelkern, *Macromolecules* **2000**, *33*, 6094.
[34] D. VanderHart, R. Alamo, M. Nyden, M. Kim, L. Mandelkern, *Macromolecules* **2000**, *33*, 6078.
[35] R. Popli, L. Mandelkern, *J. Polym. Sci., Polym. Phys. Ed.*, **1987**, *25*, 441.
[36] M. Kennedy, A. Peacock, L. Mandelkern, *Macromolecules* **1994**, *27*, 5297.
[37] M. Kennedy, A. Peacock, M. Failla, J. Lucas, L. Mandelkern, *Macromolecules* **1995**, *28*, 1407.
[38] J. Graham, R. Alamo, L. Mandelkern, *J. Polym. Sci., Polym. Phys. Ed.*, **1997**, *35*, 213.
[39] A. Peacock, L. Mandelkern, R. Alamo, J. Fatou, *J. Mater. Sci.* **1998**, *33*, 2255.
[40] K. Nitta, A. Tanaka, *Polymer*, **2001**, *42*, 1219.
[41] K. Nitta, M. Takayanagi, *J. Macromol. Sci., Part B* **2003**, *B42*, 107.
[42] S. Hosoda, A. Uemura, *Polymer J.*, **1992**, *24*, 939.
[43] S. Hosoda, *Makromol. Chem.* **1984**, *185*, 787.
[44] S. Hosoda, *Trends in Polymer Science* **1993**, *3*, 265.
[45] R. Patel, K. Sehanobishi, P. Jain, P. Chum, G. Knight, *J. Appl. Polym. Sci.* **1996**, *60*, 749.
[46] Y.-L. Huang, N. Brown, *J. Polym. Sci., Polym. Phys. Ed.*, **1991**, *29*, 129.
[47] J. Smith, K. Brzinska, D. Valenti, K. Wagener, *Macromolecules* **2000**, *33*, 3781.
[48] J. Sworen, J. Smith, J. Berg, K. Wagener, *J. Amer. Chem. Soc.* **2004**, *126*, 11238.
[49] W. Qiu, J. Sworen, M. Pyda, E. Nowak-Pyda, A. Habenschuss, K. Wagener, B. Wunderlich, *Macromolecules* **2006**, *39*, 204.
[50] J. Sworen, K. Wagener, *Macromolecules* **2007**, *40*, 4414.
[51] G. Rojas, E. Berda, K. Wagener, *Polymer* **2008**, *49*, 29.
[52] G. Rojas, T. Baughman, K. Wagener, *Synthetic Commun.* **2007**, *37*, 3923.
[53] G. Rojas, K. Wagener, *JOC* **2008**, *73*, 4962.
[54] E. Berda, T. Baughman, K. Wagener, *J. Polym. Sci. Polym. Chem. Ed.*, **2006**, *4*, 4981.

Copyright © 2009 Wiley-VCH Verlag GmbH & Co. KGaA, Weinheim

[55] H. Sano, T. Usami, H. Nakagawa, *Polymer* **1986**, *27*, 1497.
[56] R. Alamo, K. Jeon, R. Smith, E. Boz, K. Wagener, M. Bockstaller, *Macromolecules* **2008**, *41*, 7141.
[57] T. Seto, T. Hara, K. Tanaka, Japan, *J. Appl. Phys.* **1968**, *7*, 31.
[58] K. Russel, B. Hunter, R. Heyding, *Polymer* **1997**, *38*, 1409.
[59] B. Goderis, M. Basiura, V. B. F. Mathot, J. Sworen, K. Wagener, *23rd European Crystallographic Meeting, ECM23, Leuven, 2006, Acta Cryst.*, **2006**, A62, s263.

Copyright © 2009 Wiley-VCH Verlag GmbH & Co. KGaA, Weinheim